JOURNAL OF GEOPHYSICAL RESEARCH, VOL. 113, E11006, doi:10.1029/2008JE003080, 2008

Application of an adaptive least squares correlation algorithm for stereo matching planetary image data

Sarah L. André,[1] Troy C. André,[2,3] Thomas R. Watters,[1] and Mark S. Robinson[4]

Received 20 January 2008; revised 30 June 2008; accepted 14 August 2008; published 11 November 2008.

[1] An adaptive least squares (ALS) correlation algorithm and a region-growing algorithm were implemented into a stereo-matching computer program. This program (referred to as the Stereo Matching Tool Kit (SMTK)) was designed specifically for the application to planetary image data. The ALS algorithm matches a patch of one image to the corresponding area in a second image. The matching procedure is an iterative process that minimizes the sum of the square differences between the two patches to determine an optimal set of transformation parameters. Successful matches are then used to predict potential match points for surrounding locations. Using potential match points in conjunction with the region-growing algorithm, a population of match points between the two images is determined. The stereo-matching process is initiated by using the ALS algorithm in conjunction with Spacecraft, Planet, Instrument, C-matrix, and Events (SPICE) information to automatically determine a set of seed points. SMTK was tested on two planetary image data sets: Mariner 10 and Clementine. SMTK-derived digital elevation models compare well with topography generated by an area-based stereo matcher requiring manual selection of seed points, analog stereo techniques, and photoclinometry.

Citation: André, S. L., T. C. André, T. R. Watters, and M. S. Robinson (2008), Application of an adaptive least squares correlation algorithm for stereo matching planetary image data, *J. Geophys. Res.*, *113*, E11006, doi:10.1029/2008JE003080.

1. Introduction

[2] Digital elevation models (DEMs) are invaluable products for planetary terrain interpretation. For example, planetary studies of long-wavelength topography can be used with gravity data to determine crustal structure [e.g., *Zuber et al.*, 2000], while short-wavelength topography can be used to estimate strain across tectonic features [e.g., *Watters et al.*, 1998], estimate styles and magnitude of volcanism [e.g., *Sakimoto et al.*, 2002], and constrain mechanics of crater impact and modification [e.g., *Garvin et al.*, 2000]. Such studies require reliable topographic measurements typically obtained either through laser altimetry or stereo photogrammetry. Global high-resolution laser altimetry has been obtained for Mars by the Mars Orbiter Laser Altimeter [e.g., *Smith et al.*, 1998] on Mars Global Surveyor; however, spacecraft missions without laser altimeters (such as Mariner 10 for Mercury) have stereo data that have not yet been fully utilized because of the lack of a reliable and user-friendly stereo-matching tool. Thus, these studies require stereo-matching software that can reliably generate DEMs from planetary stereo images.

[3] This paper presents a method for generating DEMs from planetary science stereo images. The method consists of three steps (Figure 1): (1) an adaptive least squares (ALS) algorithm and a region-growing algorithm utilized to perform the stereo-matching process; (2) the application of the camera model to determine elevations for each matched point; and (3) the plotting of the latitude, longitude, and relative elevation values to produce a final DEM product. The software is written to work within Integrated Software for Imagers and Spectrometers (ISIS) version 2.1 [i.e., *Gaddis et al.*, 1997], a processing system common to the planetary science community, and on the Linux operating system. The application of this technique to two planetary data sets and examples of the resulting DEMs are presented in detail in sections 3.1 and 3.2.

[4] Subsequent goals of this work include making the software product available to the planetary community for use with a wide variety of image data sets. The software was designed specifically for Mariner 10 image data but has also been tested on Clementine data. Additional developments will be needed for the software to work on other data sets: for example, both the Mariner 10 and Clementine missions used framing cameras; push broom camera sensor models would need to be added for more recent missions and cameras such as the High Resolution Imaging Science Experiment (HiRISE) camera. Currently, the software functions in ISIS 2.1 and is being ported to the new version of ISIS (ISIS 3). The current version of the software (code and

[1] Center for Earth and Planetary Studies, National Air and Space Museum, Smithsonian Institution, Washington, D. C., USA.
[2] Formerly at Department of Physics, University of Chicago, Chicago, Illinois, USA.
[3] Now at Bethesda, Maryland, USA.
[4] School of Earth and Space Exploration, Arizona State University, Tempe, Arizona, USA.

0148-0227/08/2008JE003080$09.00

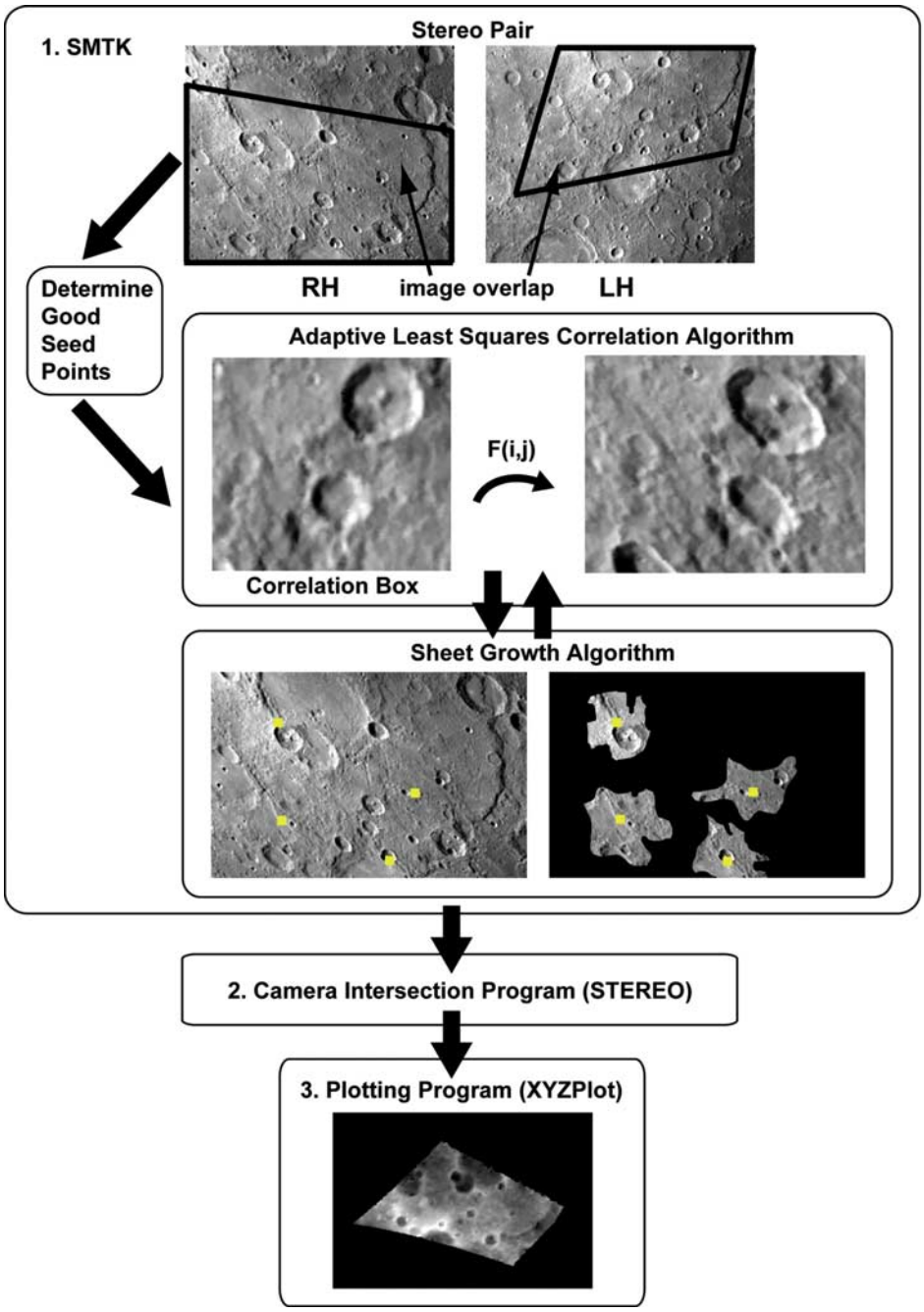

Figure 1. A flowchart diagram showing the stereo-matching process (SMTK). In step 1, the stereo-matching process initiates by identifying areas of overlap between two stereo images. Then the ALS algorithm, in conjunction with SPICE information, automatically determines a set of seed points. The ALS algorithm matches a patch of one image to the corresponding area in a second image. The matching procedure is an iterative process that minimizes the sum of the square differences between the two patches to determine an optimal set of transformation parameters. Successful matches are then used to predict potential match points for surrounding locations. Using potential match points in conjunction with the region-growing algorithm, the remaining match points between the two images are determined. In step 2, the stereo intersection program uses SPICE information and ray tracing techniques to determine the latitude, longitude, and elevation of each matched point. In step 3, the final program uses a bilinear interpolation routine to plot the latitude, longitude, and elevation of each point and produce a continuous DEM.

executables) can be freely obtained by contacting the authors. Once ported to ISIS 3 and tested, SMTK will be freely released as part of the ISIS system and will be available from and maintained by the U.S. Geological Survey.

2. Methods

[5] The Stereo Matching Tool Kit (SMTK) is composed of three distinct components: the matching software (MATCHER), the stereo camera software (STEREO), and the plotting routine (XYZPLOT) [*André et al.*, 2003, 2004]. For two overlapping images, MATCHER determines the corresponding points within the two images. Using the output of MATCHER and camera positions and orientations, STEREO determines the latitude, longitude, and relative elevation of each overlapping point. XYZPLOT uses the output of STEREO to construct the DEM.

[6] SMTK was written as a set of ISIS programs and requires the use of Spacecraft, Planet, Instrument, C-matrix, and Events (SPICE) kernels. SPICE is a system implemented by the Navigation and Ancillary Information Facility group at the Jet Propulsion Laboratory that includes ancillary data files specific to each spacecraft mission and software that can be used to calculate spacecraft position and camera orientation [*Acton*, 1996]. In sections 2.1–2.3, each of the primary components of SMTK is discussed.

2.1. MATCHER

[7] Automated digital stereo matching finds the corresponding points in two images: the reference image (left-hand image (LH)) and a right-hand image (RH). Matched points are determined by searching for patterns of pixels from the LH image in the RH image. Many stereo-matching programs require a user-selected set of homologous points (seed points) in the LH and RH images to initiate automated matching [e.g., *Day et al.*, 1992], a step that can be tedious and time consuming [i.e., *Allison et al.*, 1991]. Using the manually selected seed points, digital stereo matchers then automatically find all remaining matching points between the two images. In the MATCHER routine of SMTK, both the seed point generation process and the secondary matching step are fully automated, eliminating the need for human interaction (and potential error) in manually choosing seed points.

[8] MATCHER initially determines a preliminary set of seed points. This preliminary set of seed points consists of a grid of points in the LH image and their inferred matched points in the RH image. MATCHER estimates an initial position in the RH image on the basis of the latitude and longitude of the LH image seed point (using SPICE information). In general, the matched seed points determined using SPICE should directly correspond (in pixel space); however, error in spacecraft position and orientation often causes shifts in the position of a point in the RH image relative to the LH image. Depending on the error in camera position and orientation, the predicted matched point based on SPICE information can be off from 1 to 5 pixels for the Mariner 10 and Clementine data (this offset is data set–dependent). In order to refine the list of seed points, each pair of matched points in the grid is run through an adaptive least squares algorithm.

[9] ALS algorithms have been used as the core of stereo-matching routines for a number of years [*Gruen*, 1985; *Otto and Chau*, 1989; *Day et al.*, 1992]. ALS algorithms, like the Gruen algorithm [*Gruen*, 1985], are used to determine matched points by minimizing a goal function that measures the distance between the gray levels in a LH and a RH image patch. In equation (1), we illustrate how the goal function, Δ^2, is constructed. The goal function is the squared sum of the difference between a LH image patch and a RH image patch:

$$\Delta^2 = \sum_{i,j} \left(P_{ij}^{\mathrm{LH}} - P_{ij}^{\mathrm{RH}} \right)^2, \tag{1}$$

where P_{ij}^{LH} and P_{ij}^{RH} are the gray level values of the ijth pixel in the LH and RH image patches, respectively (i and j correspond to sample and line). The LH image patch is a correlation box centered about the proposed seed point in the LH image. The RH image patch is a resampled correlation box centered about the proposed seed point in the RH image. Resampling of the RH image patch via image-shaping parameters and radiometric corrections (both multiplicative and shift parameters) help correct for deformations in the image (e.g., elongation and shearing) and generally improve the effectiveness of the ALS algorithm. In SMTK, affine transformations are used to shape the image:

$$\begin{pmatrix} s \\ l \end{pmatrix} = \begin{pmatrix} a_{11} & a_{12} \\ a_{21} & a_{22} \end{pmatrix} \begin{pmatrix} s^0 \\ l^0 \end{pmatrix} + \begin{pmatrix} b_1 \\ b_2 \end{pmatrix}, \tag{2}$$

where (s^0, l^0) is the sample and line number of a pixel in the resampled correlation box, (s, l) is the corresponding pixel coordinates in the right-hand image patch, and a_{ij} and b_i are the affine parameters. Physically, one may view the affine transformation of equation (2) as a linear combination of four elementary operations: rotation, translation, scaling, and shearing.

[10] For a given seed point pair, the ALS algorithm in MATCHER iteratively determines the set of affine and radiometric parameters that minimize the goal function. If the ALS algorithm converges, then the affine parameters are used to construct a refined seed point pair. The ALS algorithm converges if the absolute value of the shifts in each of the affine parameters is smaller than predefined convergence thresholds (note that a user may redefine the convergence thresholds). The refined seed point pair is only used if the ALS algorithm converges and if the pair passes a set of quality constraints. Quality constraints (discussed below) are used to ensure that the matched point did not stray too far from the point predicted by the SPICE information. Sometimes the ALS routine may have a tendency to drift too far from the correct match point; this effect is most pronounced in flat regions of the image. If the ALS routine converges and passes the set of quality parameters, then the refined seed points are added to the finalized list for the region-growing algorithm. If the ALS routine fails, then the potential seed pair is removed from the list.

[11] After the final set of seed points is determined, the remaining points in the images are matched via a region-

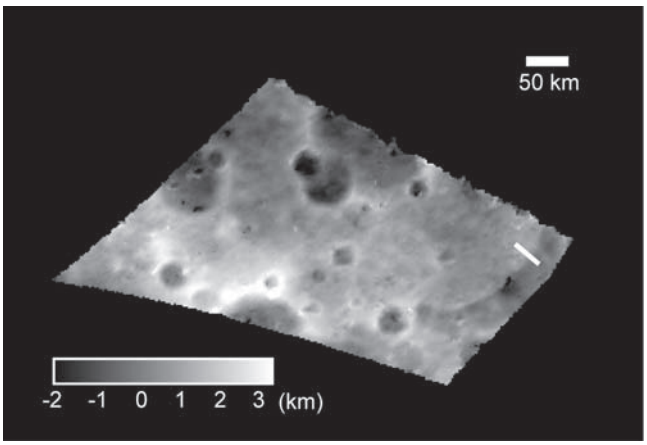

Figure 2. An example of a DEM generated by SMTK from a Mariner 10 stereo image pair (also seen in Figure 1) (images 0027399 and 0166613) in a region (50.9°–61.0°S, 35.3°–36.8°W) located in the Discovery quadrangle of Mercury. This DEM was generated using a correlation box size of 21 pixels × 21 pixels. On a 3 GHz Pentium 4 PC running Linux, this stereo pair was completed (MATCHLS, STEREO, and XYZPLOT) in 3 min and 20 s. The spatial resolution of the DEM is 2 km, and the pixel match error is estimated at ±0.05 km. Heights vary from −1.3 to 3.5 km above a reference sphere of 2439.7 km radius. The white line indicates the location of the profiles shown in Figure 5.

growing algorithm [*Otto and Chau*, 1989]. Using seed points and the affine transformation parameters, the region-growing algorithm predicts nearby match points. The ALS algorithm is then used to refine the match. If the match converges within the ALS algorithm, the match is considered good and the program continues on to the next neighboring point. Predicted match points are prioritized within the list that is used by the region-growing algorithm, and match points with low errors (i.e., small eigenvalues) from the ALS routine are matched first.

[12] Quality constraints are specified within the program to minimize the number of poor matches. These parameters can be redefined by the user to optimize the matching on the basis of the specific characteristics of the data set and the type of terrain. Some initial investigation is required by the user to determine the specific parameters beyond the default values. The stereo matcher routine has five main constraints: (1) the number of seed points determined by the automated seed point generator, (2) the size of the correlation window, (3) the grid spacing (sampling interval) in pixels in the image sample and line directions, (4) a distance tolerance based on how far a predicted matched point can vary from the SPICE-estimated location, and (5) a tolerance that restricts shifts in the x and y directions.

2.2. STEREO

[13] STEREO uses the output of MATCHER (the location of a matched point in the LH image and the corresponding subpixel location in the RH image) to determine the three-dimensional coordinates (latitude, longitude, and height) for all matched points. Spacecraft ephemeris (camera positions and orientation data) information from the mission is processed in SPICE, which is then utilized by a stereo intersection routine. Within this routine, a ray intersection method is used to solve collinearity equations and determine the point of intersection of two rays at the planetary surface [i.e., *Kraus and Waldhausl*, 1998]. The sample and line values from MATCHER are turned to planetocentric x, y, and z positions, which can then be converted into longitude, latitude, and elevation for each matched point.

2.3. XYZPLOT

[14] XYZPLOT performs a grid point interpolation of the output of STEREO (the latitude, longitude, and elevation of the matched points) to create a DEM. Any gaps between the coordinates generated from STEREO are filled in using a bilinear interpolation program. XYZPLOT creates a DEM at the same resolution as the LH image. The elevation (relative to mean radii) values are mapped into a simple cylindrical projection.

3. Application to Planetary Data and Error Assessment

[15] In this section, we discuss the application of the stereo-matching software to two specific planetary data sets, Mariner 10 and Clementine. Following these examples is a discussion of error and the accuracy of the relative heights output of the stereo-matching software.

3.1. Mariner 10 Stereo Pairs

[16] Over 2000 useful images were acquired by the Mariner 10 spacecraft during three flyby encounters in 1974 and 1975 [*Murray and Burgess*, 1977; *Spudis and Guest*, 1988]. The Mariner 10 imaging system consisted of two framing vidicon cameras (cameras A and B) with focal lengths of 1493.6 and 1500.1 mm [cf. *Robinson et al.*, 1999]. Image resolution varied depending on the flyby but was generally at 1–1.5 km [*Strom et al.*, 1975; *Spudis and Guest*, 1988].

[17] The combination of similar lighting geometries between the three flybys and the overlap in image coverage from different viewing geometries between the first and second flybys allows for excellent stereoscopy potential [*Strom et al.*, 1975; *Spudis and Guest*, 1988]. However, little stereo analysis was performed at the time of the flybys. Recently, new camera pointing and spacecraft position estimates provide an improved control network for Mercury

Table 1. Overview of the Mariner 10 Stereo Image Pair and the Resulting DEM[a]

Mariner 10	Images 0027399 and 0166613
Stereo image resolution	420 and 670 m/pixel
DEM resolution	2000 m
Number of pixels matched	348,000
Root-mean-square error	∼160 m
Pixel match error	50 m
Time to run	3 min and 20 s
Area matched	∼116,000 km^2

[a]Root-mean-square error is based on comparing a DEM profile to a photoclinometric profile. Pixel match error refers to height error based on shifting the affine parameters within SMTK (see text). Time to run indicates the amount of time that it took to run the stereo pair through SMTK (MATCHLS, STEREO, and XYZPLOT) and to create a DEM in ISIS 2.1 on a 3 GHz Pentium 4 PC running Linux.

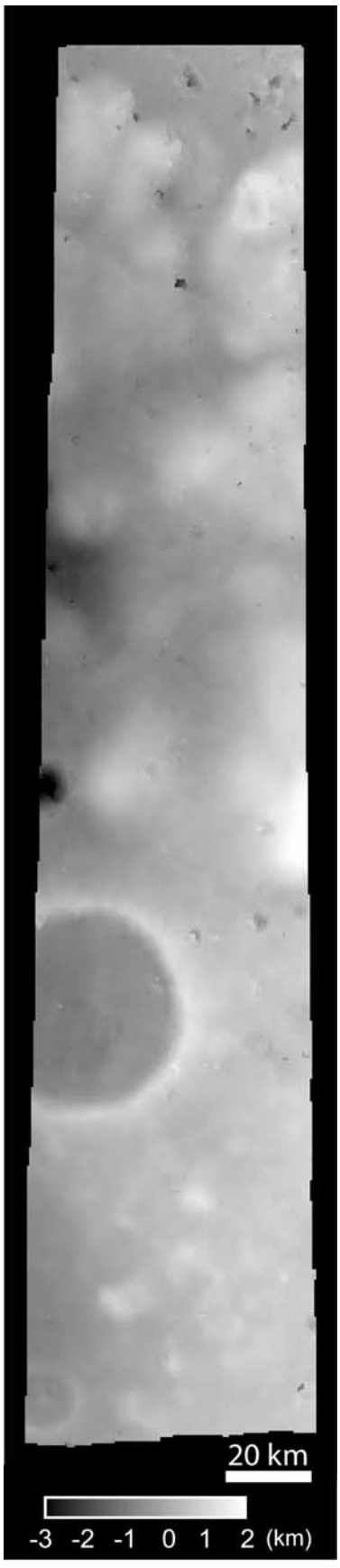

and, thus, improve the SPICE information for the Mariner 10 spacecraft [*Robinson et al.*, 1999]. With this new control network, *Cook and Robinson* [2000] determined the amount and quality of useable stereo coverage for Mercury. Topographic data derived from Mariner 10 stereo pairs (generated using a version of Gotcha, a stereo matcher created at University College London [*Day et al.*, 1992] requiring manually selected seed points) have been used to measure the relief of tectonic landforms such as lobate scarps and high-relief ridges, to constrain models for the geometry and depth of faulting, and to identify a previously unrecognized impact basin [*Watters et al.*, 1998, 2001, 2002, 2004]. We continue the stereo analysis project for Mercury using SMTK to perform the DEM generation because it can rapidly and accurately process the Mariner 10 stereo pairs. Preprocessing (independent of the stereo-matching software) of the raw Mariner 10 images includes using existing ISIS routines to identify and remove reseau, perform photometric calibration, remove noise, and correct geometric distortion.

[18] The images shown in Figure 1 are a good example of the better stereo coverage obtained in the Mariner 10 flybys (image frames 0027399 and 0166613). The stereo pair has a large area of overlap between the two images, and the resolution of the images is roughly comparable (420 and 670 m/pixel, respectively). The individual DEM (in Figure 2 and described in Table 1) was constructed using 100 seed points, a correlation box size of 21 pixels $\times$ 21 pixels, a grid spacing of 3 pixels $\times$ 3 pixels, a distance cutoff of 8 pixels, and a shift cutoff in the x and y directions of 0.5 pixels. On a 3 GHz Pentium 4 PC running Linux, this stereo pair was completed (MATCHLS, STEREO, and XYZPLOT) in 3 min and 20 s. The spatial resolution of the DEM is 2 km. The pixel match error is estimated at $\pm$0.05 km. The DEM covers an area $\sim$450 km across and $\sim$300 km wide located in the southern hemisphere (50.9°–61.0°S, 35.3°–36.8°W). Heights vary from $-$1.3 to 3.5 km above a reference sphere of 2439.7 km. The prominent curvilinear landform is Discovery Rupes, a large-scale lobate scarp.

3.2. Clementine Stereo Pairs

[19] The Clementine spacecraft was a polar orbiter that completed global multispectral mapping of the lunar surface in 1994 [*Nozette et al.*, 1994; *McEwen and Robinson*, 1997]. About 600,000 ultraviolet-visible images were

Figure 3. A regional DEM consisting of 11 Clementine lunar stereo image pairs, including the nadir-pointing images (lub2309h–lub2441h) from orbit 333 and the tilted-pointing images (lub1778h–lub1884h) from adjacent orbit 338. Each DEM was constructed using a correlation box size of 17 pixels $\times$ 17 pixels. On a 3 GHz Pentium 4 PC running Linux, a single Clementine stereo pair was completed (MATCHLS, STEREO, and XYZPLOT) in 25 s. The spatial resolution of the DEM is 1 km, and the pixel match error is $\pm$0.100 km. The region shown is located near the eastern region of the rings of Orientale Basin (20°S, 95°W). Heights vary from $-$2.8 to 1.2 km (relative to the 1737.4 km radius reference sphere). Crater Kopff (17.5°S, 270.6°W), the largest crater in the DEM, has a diameter of 42 km.

Table 2. Overview of a Clementine Stereo Image Pair and the Resulting DEM[a]

Clementine	Images lub1778h.338 and lub2309h.333
Stereo image resolution	190 and 150 m/pixel
DEM resolution	1000 m
Number of pixels matched	81,945
Root-mean-square error	~130 m
Pixel match error	100 m
Time to run	25 s
Area matched	~1918 km^2

[a]Root-mean-square error is based on comparing a Clementine DEM profile to a LTO profile. Pixel match error refers to height error based on shifting the affine parameters within SMTK (see text). Time to run indicates the amount of time that it took to run the stereo pair through SMTK (MATCHLS, STEREO, and XYZPLOT) and to create a DEM in ISIS 2.1 on a 3 GHz Pentium 4 PC running Linux.

obtained using a geometrically and radiometrically precise charge-coupled device framing camera [*Nozette et al.*, 1994; *Cook et al.*, 2000]. Special stereo sequences were acquired during the end of the mapping mission; however, the majority of stereo imagery occurs as simple overlap from the global nadir-pointing images between adjacent orbits [cf. *Cook et al.*, 2000]. Initial processing of the raw Clementine images included radiometric calibration using standard ISIS routines. One of the special stereo sequences (with adjacent orbits of nadir-pointing and off-nadir images) was obtained along the eastern interior rim of Orientale Basin (20°S, 95°W). A DEM of this area was constructed previously using another stereo matcher [*Oberst et al.*, 1996], making it particularly useful for comparison with a DEM generated by SMTK.

[20] Figure 3 shows a mosaic of the Clementine DEMs derived from 11 nadir-pointing images (lub2309h–lub2441h) from orbit 333 and 11 corresponding off-nadir images (lub1778h–lub1884h) from orbit 338. Images have a spatial resolution of ~150 m/pixel. An overview of one of the Clementine stereo image pairs and the resulting DEM is described in Table 2. The 11 individual DEMs were each constructed using 100 seed points, a correlation box size of 17 pixels × 17 pixels, a grid spacing of 3 pixels, a distance cutoff of 8 pixels, and an x and y shift of 1.0 pixel. On a 3 GHz Pentium 4 PC running Linux, a single Clementine stereo pair was completed (MATCHLS, STEREO, and XYZPLOT) in 25 s. The DEM covers an area 270 km × 50 km and has a spatial resolution of 1 km. The pixel match error is estimated at ±0.10 km (see discussion in section 3.3). Heights vary from +1200 to −2800 m (relative to the 1737.4 km radius reference sphere). The 42 km diameter Kopff crater (17.5°S, 270.6°W), the largest crater in the DEM, is 2 km deep. The smaller crater, Kopff E, has a depth of 2.9 km.

3.3. Error Assessment

[21] To provide a qualitative measure of the lateral quality and resolution of the SMTK DEM, we compare the nadir-pointing Mariner 10 image and a shaded relief representation of the SMTK DEM (Figure 4). The shaded relief image computed from the DEM emphasizes local detail, providing a visual impression of what features are and are not resolved and what sort of artifacts and noise are present within the DEM. In general, the shaded relief representation of the SMTK DEM is consistent with the gray value image and gives a good impression of the quality of the DEM. In the example shown in Figure 4, the shaded relief representation of the DEM (created with a 21 pixel × 21 pixel correlation box size) shows that craters smaller than 10 km in diameter are absent (not resolved) and craters between 10 and 15 km diameter are present but poorly resolved. Craters larger than 15 km in diameter are well resolved.

[22] In general, the sources and magnitude of the error in stereo-based measurements depend on the specific stereo-matching algorithm and the characteristics of the image data set; software can be limited by factors such as images with high noise and low signal, shadows, and extremes in parallax. Two major sources of error for the Mariner 10 and Clementine data sets are inaccurate camera position and pointing (SPICE) information and image noise caused by instrumental defects or cosmic ray hits. Inaccurate SPICE information can affect the seed point generation process, the stereo-matching process, and the region-growing algorithm. Some image data sets (such as Mariner 10) generally have low signal-to-noise ratios. The widespread image noise is difficult to completely filter from the images. This noise can affect the matching process by creating mismatches or other subpixel errors.

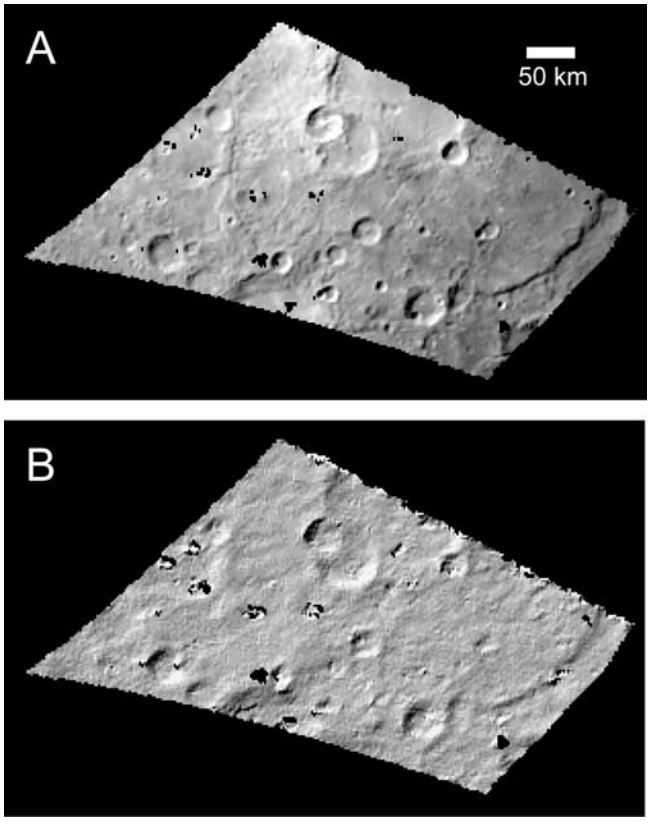

Figure 4. (a) A Mariner 10 image (image 0166613) and (b) the shaded relief representation of the SMTK DEM (stereo pair 0027399 and 0166613) for comparison. The shaded relief representation is generally consistent with the Mariner 10 image. In the shaded relief representation, craters between 10 and 15 km in diameter are present but poorly resolved, and craters less than 10 km in diameter are absent.

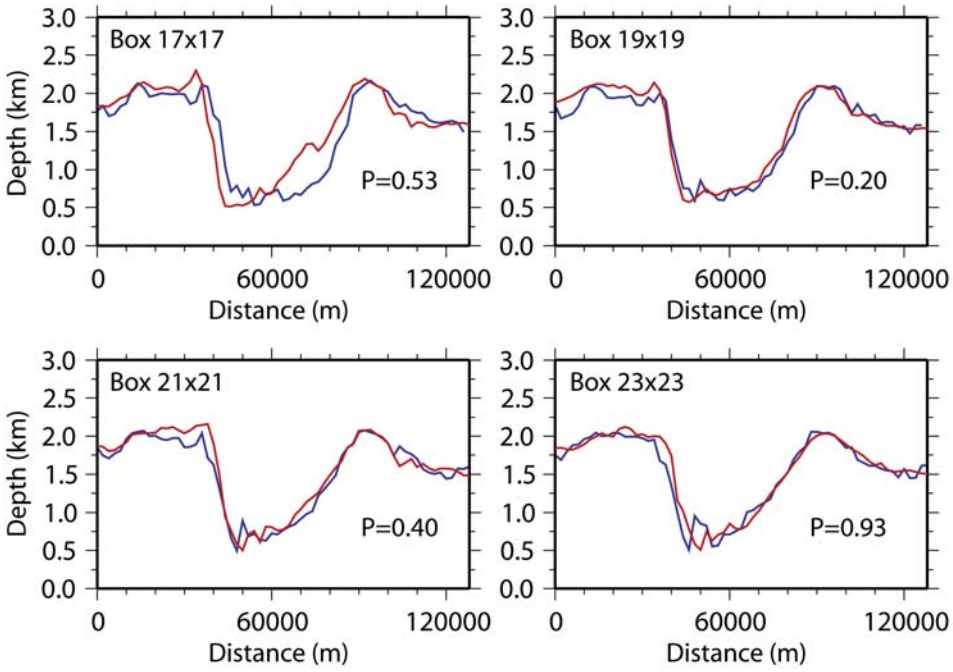

Figure 5. A comparison of a topographic profile across the same feature from a Mariner 10 DEM generated by SMTK (blue profile) and the DEM generated by the Gotcha stereo-matching program (red profile) [*Day et al.*, 1992]. The profile is taken from the DEM shown in Figure 2. Profiles from each of four correlation box sizes (17 pixels × 17 pixels, 19 pixels by 19 pixels, 21 pixels × 21 pixels, and 23 pixels × 23 pixels) are shown. Visually comparing the profiles shows that the data consistently agree. The K-S statistical test was performed for each box size, with *P* indicating the probability that the two data sets agree. The *P* results are listed in the graph for each box size. Even though the profiles for each box size visually agree, in some instances noise in the profile can affect the results of the K-S test and result in a low *P* value.

[23] To better understand how error is estimated by SMTK, we separate the discussion of error into two parts on the basis of the final output of the software: the unmatched areas and the matched areas within a resulting DEM. In SMTK, the error in the matched regions is estimated using the error in the ALS routine for each matched point. For each point, SMTK calculates the eigenvalue that indicates the error in the affine shift parameters, δb_1 and δb_2 (see equation (2)). To determine the extent of this error, the algorithm is rerun and allowed to converge within the new shift parameters; thus, the eigenvalue is used to calculate a new set of matched points. Then, with the new set of matched points, SMTK uses STEREO and XYZPLOT to determine a new height. The difference between the original height and the parameter shift height is considered to be the pixel match error for that matched point. The height difference is determined for each matched point within the stereo pair. The average elevation difference represents the pixel match error of the stereo pair.

3.3.1. Unmatched Areas

[24] The stereo-matching algorithm is sometimes unable to converge to a match, thus creating areas of no data within a DEM (seen as black areas or holes). In general, the stereo-matching algorithm may have difficulty in matching areas with the same or similar digital number (DN) values (areas with low contrast). This type of problem typically corresponds to terrain that is relatively devoid of features (i.e., smooth and flat). In addition to areas that cannot be matched, mismatches within the DEM (referred to as blunders) result either from incorrect matches of different features (typically whole pixel errors) or from almost correctly matched features (typically subpixel errors). Most of the time blunders will not be accepted because of the user's choice of quality constraints and are thrown out. Some, however, fall within the quality constraints and can be seen visibly. Blunders appear as small areas with higher DN values relative to other areas in the DEM. In the case of the Mariner 10 data set, most blunders are due to the stereo-matching algorithm attempting to match the image noise. Adjusting the user-input parameters may in some cases lessen the areal extent of the blunders but rarely completely eliminates them.

3.3.2. Matched Areas

3.3.2.1. Comparison With Other Stereo Matcher Results

[25] To better understand the potential error associated with the successfully matched points of the DEMs generated by SMTK, we compare our results to those from other stereo matchers. To evaluate the error of successfully matched points, SMTK results for a specific stereo pair were compared to those generated from the Gotcha matcher. Gotcha is also based on an adaptive least squares algorithm and is reported to be reliable and to have high accuracy [*Gruen*, 1985; *Otto and Chau*, 1989; *Day and Muller*, 1989; *Day et al.*, 1992]. Ten topographic profiles were extracted from corresponding areas within

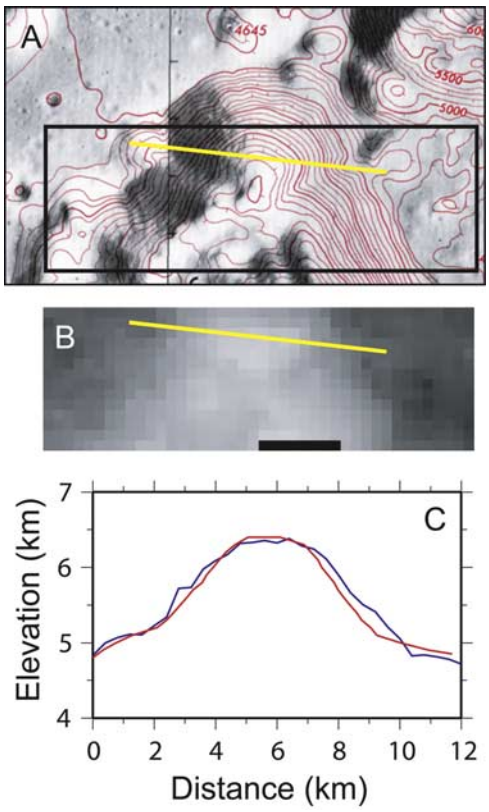

Figure 6. (a) A section of the Vitruvius region of the Moon (map adapted from the lunar topographic orthophotomap LTO-43D4), an area south of the Apollo 17 landing site [*NASA*, 1974]. The contours are at 100 m intervals, spot elevations are noted in red text, and the map has a vertical accuracy of ±31 m [*NASA*, 1974]. Elevations are shown relative to 1730 km lunar radius reference. (b) The Clementine DEM (derived from the image pair lub3274l and lub3241k from orbit 289) of the section of Mons Vitruvius (19.6–19.8°N, 30.9–31.4°E) shows the location of the extracted profile. The spatial resolution of the DEM is 1 km, and the pixel match error is ±0.100 km. (c) The profiles extracted from the LTO (red curve) and the DEM (blue curve) indicate good agreement (a correlation coefficient of 0.90 and a RMSE of 0.130 km). The black rectangle shows the area seen in Figure 6b, and the yellow lines indicate the location of the profiles seen in Figure 6c.

SMTK and Gotcha-produced DEMs for four different correlation box sizes, 17 pixels × 17 pixels, 19 pixels × 19 pixels, 21 pixels × 21 pixels, and 23 pixels × 23 pixels (see example in Figure 5). In general, DEMs created with smaller correlation box sizes are subject to more high-frequency noise, while DEMs created with larger correlation box sizes are subject to topographic smoothing. In order to quantify the agreement between DEMs, we compared the profiles from SMTK and Gotcha using two methods: the correlation coefficient and the Kolmogorov-Smirnov (K-S) test. We computed the correlation coefficient for the 10 different profile pairs for each correlation box size. The average correlation coefficient for the 10 profiles is 0.93, thereby indicating good agreement between the SMTK and Gotcha sets of profiles.

[26] The K-S test [i.e., *D'Agostino and Stephens*, 1986] was also used to test the hypothesis that a profile from the SMTK DEM and the corresponding profile from the Gotcha DEM have the same shape (i.e., are drawn from the same distribution). The K-S test is a nonparametric statistical test that can be used to determine goodness of fit between two data sets. The profiles are converted to a cumulative probability distribution, and then the absolute maximum difference between the SMTK data and the Gotcha data is computed. The calculated probability, P, from the K-S test indicates if the two data sets differ appreciably. If P is low, then reject the null hypothesis that the two data sets are from the same distribution, and if P is high, then accept the null hypothesis. A disadvantage to the K-S test is its sensitivity to outliers. Thus, if the profile had some spikes related to noise, the K-S test would result in a low P (low probability of agreement between the two data sets). For the larger correlation box sizes (19 pixels × 19 pixels, 21 pixels × 21 pixels, and 23 pixels × 23 pixels) more than half of the SMTK data agrees at a $P = 60\%$ or higher with the Gotcha data. The smallest correlation box size (17 pixels × 17 pixels) shows less agreement because profiles taken at this correlation box size are subject to more noise. However, visual observations of profiles from the 17 pixel × 17 pixel correlation box size indicate that except for the spurious noise (outliers) the data appear to agree between DEMs. In general, the shape of the SMTK data shows good agreement with the Gotcha data, thus indicating that the two methods are comparable.

[27] SMTK results were also compared to point results of a similar Clementine DEM constructed by the group at the Institute of Planetary Exploration as part of the Deutsches Zentrum für Luft- und Raumfahrt (DLR), which developed its own set of stereo image processing techniques [*Oberst et al.*, 1996, 1997]. The DLR group determined that the crater Kopff (17.5°S, 270.6°W) is about 2.2 km deep and crater Kopff E is 3.1 km deep with respect to a lunar reference sphere of 1737.4 km in radius. Height accuracy on the DEMs created by the DLR matcher for this region of the Moon is ±0.100 km [*Cook et al.*, 1996; *Oberst et al.*, 1996]. The DLR measurements are consistent (within the error) with those from the DEM generated by SMTK, 2 and 2.9 km, respectively (±0.100 km).

[28] Additionally, topographic results from a Clementine DEM generated by SMTK were compared to those from a NASA lunar topographic orthophotomap (LTO). The LTO series of topographic maps were generated from Apollo 15, 16, and 17 panoramic camera and metric camera stereo images, have contour intervals of 100 m, and include some spot elevations [i.e., *Schimerman*, 1973]. We extracted a profile from LTO-43D4, which shows the Vitruvius region of the Moon, located to the north of Mare Tranquillitatis and to the southeast of Mare Serenitatis [*NASA*, 1974]. The LTO was generated from Apollo 17 images and has an estimated vertical accuracy of ±31 m [*NASA*, 1974]. A profile was extracted along the northern edge of Mons Vitruvius, a mountain range south of the Apollo 17 landing site. The Clementine DEM was derived from the image pair lub3274l and lub3241k from orbit 289. The images have a spatial resolution of ~106 m/pixel. The DEM was constructed using 100 seed points, a correlation box size of 17 pixels × 17 pixels, a grid spacing of 3 pixels, a distance cut of

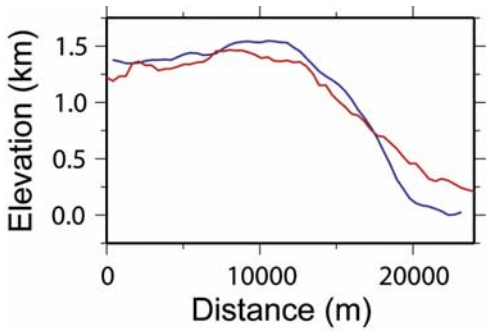

Figure 7. The topographic profiles extracted from photoclinometry (red curve) and the SMTK DEM (blue curve) across Discovery Rupes on Mercury. The maximum relief of the scarp as determined in the DEM is 1.3 ± 0.050 km, which concurs with the photoclinometric results of 1.5 ± 0.2 km [*Watters et al.*, 1998]. The correlation coefficient for the two profiles is 0.98, indicating good agreement between the two methods.

2 pixels, and an x and y shift of 0.5 pixels. The spatial resolution of the DEM is 1 km, and the pixel match error is ±0.100 km. The root-mean-square error (RMSE) is a measure of the vertical height error and is calculated by determining the difference between corresponding points on the curves, squaring the differences, dividing by the number of points, and then taking the square root of the sum. The RMSE between the profiles extracted from the Clementine DEM and the Apollo LTO is 0.130 km, indicating good agreement between the profiles from the LTO and the DEM (Figure 6). In addition, a correlation coefficient of 0.90 was calculated for the profiles, also indicating good agreement.

[29] The relative depth measurements extracted from SMTK are comparable with those from two other stereo-matching programs (Gotcha and the DLR matcher) and consistent with other topographic data (such as the LTO). To further quantify SMTK results, we compare our results to those collected from other measurement techniques.

3.3.2.2. Comparison With Other Measurement Techniques

[30] Photoclinometric profiles of elevation across Discovery Rupes provide an additional independent check of the accuracy of the relative heights generated from the stereo-matching software. Photoclinometry involves the use of variations in shading to derive topography, either along a line (monoscopic photoclinometry) or an area (two-dimensional photoclinometry) [cf. *McEwen*, 1991]. *Watters et al.* [1998] used monoscopic photoclinometry on Mariner 10 images to generate topographic profiles across Discovery Rupes. They compared the photogrammetric profiles with topography obtained from the Gotcha matcher to provide an independent check of the accuracy of the DEM [*Watters et al.*, 1998]. The study determined the average relief of the scarp to be 1.3 ± 0.2 km, with a maximum relief of 1.5 km [*Watters et al.*, 1998]. The same photoclinometric profile (of the maximum relief) was compared to a profile extracted from a DEM generated from Mariner 10 images using SMTK (Figure 7). The maximum relief for the SMTK profile is 1.3 ± 0.050 km, which concurs with the photoclinometric results within the stated error. To quantify the agreement between the profile extracted from the DEM and photoclinometry, we computed the correlation coefficient; the correlation is 0.98, indicating good agreement between the two methods. The RMSE between the profile extracted from the Mariner 10 DEM and the photoclinometric profile is 0.160 km, also indicating good agreement.

[31] Crater depths measured from the Mariner 10 SMTK DEMs were compared to shadow measurements of crater depths [i.e., *Pike*, 1988]. Shadow measurements of crater depths yield accurate relative heights but are limited to craters that have shadows that reach the crater center. Four complex craters in the hemisphere imaged from Mariner 10 (in the Discovery and Bach quadrangles) can be measured using both stereo analysis and shadow measurements. A comparison of results is listed in Table 3. Measurements from DEMs generated by SMTK are consistent (within the quoted error) with the shadow measurements of crater depth.

4. Conclusions

[32] The software, Stereo Matching Tool Kit (SMTK), can (1) automatically generate seed points, (2) perform the stereo-matching process, (3) apply the camera intersection model, and (4) produce DEMs. Quality parameters can be defined by the user to optimize matching on the basis of the specific needs of the data set and the type of terrain. SMTK produces reliable DEMs from Mariner 10 and Clementine stereo images. An error assessment that includes comparisons with DEMs generated using other stereo-matching programs and topographic data derived from other measurement techniques indicates that SMTK provides accurate relative height measurements. SMTK is a user-friendly tool that could be used by others in the planetary science community on a variety of image data sets to produce automated topographic products.

[33] There are multiple advantages to having SMTK run within the ISIS framework. As suggested in section 1, ISIS is a software commonly used by the planetary science community. SMTK does not require image reformatting (it works with the standard ISIS image format) and uses the SPICE kernels within the ISIS software. MATCHLS requires a total of six parameters to be set by the user in order to find the seed points and complete the entire matching process between the stereo pair, a number of parameters comparable to many ISIS routines. In general, users will need to determine this set of parameters for the specific data set, not for each stereo pair. For example, the parameters listed for the Mariner 10 example in section 3.1 (Figure 2) were used for the majority of the Mariner 10

Table 3. Comparison of Crater Depths Determined From DEM and Shadow Measurements

Latitude (°S)	Longitude (°W)	Diameter (km)	Depth[a] (km)	
			DEM	Shadow
65.1	33.8	53	2.5 ± 0.1	2.4
66.5	30.2	70	3.5 ± 0.1	3.0
79.4	50.8	62	2.7 ± 0.2	2.5
81.2	84.7	41	2.2 ± 0.2	2.2

[a]Depths were determined from DEMs generated by SMTK and from shadow measurements of Mariner 10 images.

stereo pairs. We will provide documentation within ISIS on how best to determine the parameters for MATCHLS. ISIS users can also view and compare the resulting DEM to the stereo images using the ISIS viewer Qview, which also has the capability for a user to edit the DEM.

[34] As discussed in section 1, SMTK currently works on data from the Mariner 10 and Clementine spacecraft missions. Our hope is that SMTK can be used on other planetary missions. Additional preprocessing steps would likely need to be applied to newer planetary data sets. For example, although neither Mariner 10 nor Clementine SPICE was greatly mispositioned (SPICE was off by only 1–5 pixels), other mission data may require a preprocessing step such as bundle block adjustment to account for imprecise SPICE or extremes in parallax. In addition, Mariner 10 and Clementine are both framing camera missions, so the software would need adjustments in order to accommodate additional sensor models such as a push broom scanner model.

[35] The newest version of ISIS, ISIS 3, is a graphical user interface–based update of ISIS 2 written entirely in C++ that is designed to work with current and upcoming spacecraft missions. Currently, SMTK is under development to be ported into ISIS 3. It is our plan that SMTK be supported and maintained in the ISIS 3 environment and that it will be distributed freely in future releases of ISIS 3.

[36] **Acknowledgments.** We would like to thank Kay Edwards for her invaluable programming assistance with the STEREO and XYZPLOT routines. We also thank Anthony Cook for many useful discussions of photogrammetry and the Gotcha stereo-matching software. Anthony Cook obtained permission to use a version of the Gotcha stereo-matching software (originally written by Tim Day) from University College London and Laser-Scan. We also thank two anonymous reviewers for helpful comments and suggestions.

References

Acton, C. H. (1996), Ancillary data services of NASA's Navigation and Ancillary Information Facility, *Planet. Space Sci.*, *44*, 65–70, doi:10.1016/0032-0633(95)00107-7.

Allison, D., M. J. A. Zemerly, and J.-P. Muller (1991), *Automatic seed-point generation for stereo-matching and multi-image registration, IGARSS "91*, 2417–2421, Inst. of Electr. and Electron. Eng., New York.

André, S. L., T. C. André, and M. S. Robinson (2003), Automated extraction of planetary digital elevation models, *Eos Trans. AGU*, *84*(46), Fall Meet. Suppl., Abstract P41B-0411.

André, S. L., M. S. Robinson, and T. C. André (2004), Topographic analysis with a stereo matching tool kit, *Lunar Planet. Sci.*, *XXXV*, abstract 2057.

Cook, A. C., and M. S. Robinson (2000), Mariner 10 stereo image coverage of Mercury, *J. Geophys. Res.*, *105*, 9429–9443, doi:10.1029/1999JE001135.

Cook, A. C., J. Oberst, T. Roatsch, R. Jaumann, and C. Acton (1996), Clementine imagery: Selenographic coverage for cartographic and scientific use, *Planet. Space Sci.*, *44*, 1135–1148, doi:10.1016/S0032-0633(96)00061-X.

Cook, A. C., T. R. Watters, M. S. Robinson, P. D. Spudis, and D. B. J. Bussey (2000), Lunar polar topography derived from Clementine stereo-images, *J. Geophys. Res.*, *105*, 12,023–12,033, doi:10.1029/1999JE001083.

D'Agostino, R. B., and M. A. Stephens (1986), *Goodness-of-Fit Techniques*, 560 pp., Marcel Dekker, New York.

Day, T., and J.-P. Muller (1989), Digital elevation model production by stereo-matching spot image-pairs: A comparison of algorithms, *Image Vision Comput.*, *7*, 95–101, doi:10.1016/0262-8856(89)90002-4.

Day, T., A. C. Cook, and J.-P. Muller (1992), Automated digital topographic mapping techniques for Mars, *Int. Arch. Photogramm. Remote Sens.*, *29*(B4), 801–808.

Gaddis, L., et al. (1997), An overview of the Integrated Software for Imaging Spectrometers(ISIS), *Lunar Planet. Sci., XXVIII*, 1226.

Garvin, J. B., S. E. H. Sakimoto, J. J. Frawley, and C. Schnetzler (2000), North polar region craterforms on Mars: Geometric characteristics from the Mars Orbiter Laser Altimeter, *Icarus*, *144*, 329–352, doi:10.1006/icar.1999.6298.

Gruen, A. W. (1985), Adaptive least squares correlation: A powerful image matching technique, *S. Afr. J. Photogramm. Remote Sens. Cartogr.*, *14*, 175–187.

Kraus, K., and P. Waldhausl (1998), *Manuel de Photogrammétrie: Principes et Procédés Fondamentaux*, 407 pp., Hermes, Paris.

McEwen, A. (1991), Photometric functions for photoclinometry and other applications, *Icarus*, *92*, 298–311, doi:10.1016/0019-1035(91)90053-V.

McEwen, A., and M. S. Robinson (1997), Mapping of the Moon by Clementine, *Adv. Space Res.*, *19*, 1523–1533, doi:10.1016/S0273-1177(97)00365-7.

Murray, B., and E. Burgess (1977), *Flight to Mercury*, 162 pp., Columbia Univ. Press, New York.

NASA (1974), Lunar topographic orthophotomap, *Map LTO-43D4*, Def. Mapp. Agency Topogr. Cent., Washington, D. C.

Nozette, S., et al. (1994), The Clementine mission to the Moon: Scientific overview, *Science*, *266*, 1835–1839, doi:10.1126/science.266.5192.1835.

Oberst, J., T. Roatsch, W. Zhang, A. C. Cook, R. Jaumann, T. Duxbury, F. Wewel, R. Uebbing, F. Scholten, and J. Albertz (1996), Photogrammetric analysis of Clementine multi-look angle images obtained near Mare Orientale, *Planet. Space Sci.*, *44*, 1123–1133, doi:10.1016/S0032-0633(96)00060-8.

Oberst, J., M. Waehlisch, A. C. Cook, T. Roatsch, and R. Jaumann (1997), Lunar details gleaned from digital stereo images, *Eos Trans. AGU*, *78*(41), 445, doi:10.1029/97EO00275.

Otto, G. P., and T. K. W. Chau (1989), "Region-growing" algorithm for matching of terrain images, *Image Vision Comput.*, *7*, 83–94, doi:10.1016/0262-8856(89)90001-2.

Pike, R. J. (1988), Geomorphology of impact craters on Mercury, in *Mercury*, edited by F. Vilas, C. R. Chapman, and M. S. Matthews, pp. 165–273, Univ. of Ariz. Press, Tucson.

Robinson, M. S., M. E. Davies, T. R. Colvin, and K. Edwards (1999), A revised control network for Mercury, *J. Geophys. Res.*, *104*, 30,847–30,852, doi:10.1029/1999JE001081.

Sakimoto, S. E. H., S. S. Hughes, and T. K. Gregg (2002), Plains volcanism on Mars: Topographic data on shield and flow distributions and abundances, with new quantitative comparisons to the Snake River plain volcanic province, *Geol. Soc. Am. Abstr. Programs*, *34*(6), 173.

Schimerman, L. A. (Ed.) (1973), The lunar cartographic dossier, *NASA-CR 1464000*, U. S. Def. Mapp. Agency, St. Louis, Mo.

Smith, D. E., et al. (1998), Topography of the northern hemisphere of Mars from the Mars Orbiter Laser Altimeter, *Science*, *279*, 1686–1692, doi:10.1126/science.279.5357.1686.

Spudis, P. D., and J. E. Guest (1988), Stratigraphy and geologic history of Mercury, in *Mercury*, edited by F. Vilas, C. R. Chapman, and M. S. Matthews, pp. 118–164, Univ. of Ariz. Press, Tucson.

Strom, R. G., et al. (1975), Preliminary imaging results from the second Mercury encounter, *J. Geophys. Res.*, *80*, 2345–2356, doi:10.1029/JB080i017p02345.

Watters, T. R., M. S. Robinson, and A. C. Cook (1998), Topography of lobate scarps on Mercury: New constraints on the planet's contraction, *Geology*, *26*, 991–994, doi:10.1130/0091-7613(1998)026<0991:TOLSOM>2.3.CO;2.

Watters, T. R., A. C. Cook, and M. S. Robinson (2001), Large-scale lobate scarps in the southern hemisphere of Mercury, *Planet. Space Sci.*, *49*, 1523–1530, doi:10.1016/S0032-0633(01)00090-3.

Watters, T. R., R. A. Schultz, M. S. Robinson, and A. C. Cook (2002), The mechanical and thermal structure of Mercury's early lithosphere, *Geophys. Res. Lett.*, *29*(11), 1542, doi:10.1029/2001GL014308.

Watters, T. R., M. S. Robinson, C. R. Bina, and P. D. Spudis (2004), Thrust faults and the global contraction of Mercury, *Geophys. Res. Lett.*, *31*, L04701, doi:10.1029/2003GL019171.

Zuber, M. T., et al. (2000), Internal structure and early thermal evolution of Mars from Mars Global Surveyor topography and gravity, *Science*, *287*, 1788–1793, doi:10.1126/science.287.5459.1788.

S. L. André and T. R. Watters, Center for Earth and Planetary Studies, National Air and Space Museum, Smithsonian Institution, P. O. Box 37012, Washington, DC 20013-7012, USA. (andres@si.edu)

T. C. André, 4800 Hampden Lane, Suite 500, Bethesda, MD 20814, USA.

M. S. Robinson, School of Earth and Space Exploration, Arizona State University, P. O. Box 871404, Tempe, AZ 85287-1404, USA.